# First simulation study of trackless events in the INO-ICAL detector to probe the sensitivity to atmospheric neutrino oscillation parameters

Aleena Chacko,[1,*] D. Indumathi,[2,3,†] James F. Libby,[1,‡] and P. K. Behera[1,§]

[1]*Indian Institute of Technology Madras, Chennai 600 036, India*
[2]*The Institute of Mathematical Sciences, Chennai 600 113, India*
[3]*Homi Bhabha National Institute, Training School Complex, Anushakti Nagar, Mumbai 400085, India*

(Received 17 December 2019; accepted 30 July 2020; published 14 August 2020)

The proposed India-based Neutrino Observatory will host a 50 kton magnetized iron calorimeter (ICAL) with resistive plate chambers as its active detector element. Its primary focus is to study charged-current interactions of atmospheric muon neutrinos via the reconstruction of muons in the detector. We present the first study of the energy and direction reconstruction of the final state lepton and hadrons produced in charged current interactions of atmospheric electron neutrinos at ICAL and the sensitivity of these events to neutrino oscillation parameters $\theta_{23}$ and $\Delta m^2_{32}$. However, the signatures of these events are similar to those from neutral-current interactions and charged-current muon neutrino events in which the muon track is not reconstructed. On including the entire set of events that do not produce a muon track, we find that reasonably good sensitivity to $\theta_{23}$ is obtained, with a relative $1\sigma$ precision of 15% on the mixing parameter $\sin^2\theta_{23}$, which decreases to 21%, when systematic uncertainties are considered.

DOI: 10.1103/PhysRevD.102.032005

## I. INTRODUCTION AND MOTIVATION

The phenomenon of neutrino oscillations arises when neutrino-mass eigenstates ($\nu_1$, $\nu_2$, and $\nu_3$) coherently superpose to form neutrino-flavor states ($\nu_e$, $\nu_\mu$, and $\nu_\tau$). The mass eigenstates and flavor states are related by a $3\times 3$ unitary matrix [1], which is parametrized by three mixing angles ($\theta_{12}, \theta_{23}$, and $\theta_{13}$) and the $CP$-violating Dirac phase $\delta_{CP}$. Along with the dependence on these four parameters, the oscillation probability depends upon the mass-squared differences $\Delta m^2_{ij} \equiv m^2_i - m^2_j$, $(i \neq j)$, with $i$ and $j$ being any of the mass eigenstates. As only two of the three values of $\Delta m^2_{ij}$ are independent, oscillations are usually parametrized by $\Delta m^2_{21}$ and $\Delta m^2_{32}$. Hence, measurements of neutrino oscillations are only sensitive to the $\Delta m^2_{ij}$ and not to the neutrino masses.

Recent measurements from solar and reactor data [2] give the best-fit value of the "solar parameters" as $\sin^2\theta_{12} = 0.307^{+0.013}_{-0.012}$ and $\Delta m^2_{21} = (7.53 \pm 0.18)\times 10^{-5}\,\mathrm{eV}^2$ [3]. Furthermore, reactor $\bar{\nu}_e$ data precisely determine the mixing angle, $\theta_{13}$ [4–6]. Measurements of atmospheric and accelerator neutrinos are sensitive to the "atmospheric parameters" $\Delta m^2_{32}$ and $\theta_{23}$. While $|\Delta m^2_{32}| = 2.444 \pm 0.034 \times 10^{-3}\ \mathrm{eV}^2$ [7] has been measured, its sign, which determines the neutrino mass ordering as well as the octant of $\theta_{23}$, are currently unknown.

Current and near-future experiments [8–11] can confirm the sign of $\Delta m^2_{32}$ being positive (normal ordering or hierarchy, NH) or negative (inverted ordering or hierarchy, IH) as well as resolve the octant problem, *i.e.*, $\theta_{23} = \pi/4$ (maximal mixing), $\theta_{23} < \pi/4$ (lower octant), or $\theta_{23} > \pi/4$ (upper octant). A global analysis of neutrino-oscillation parameters [12] favors the upper octant of $\theta_{23}$, with a best fit value of $\sin^2\theta_{23} = 0.580^{+0.017}_{-0.021}$. However, the octant is still undetermined, with the $3\sigma$ range of this parameter including both octants: $0.42 \leq \sin^2\theta_{23} \leq 0.63$.

The proposed magnetized iron calorimeter (ICAL) detector at the India-based Neutrino Observatory (INO) is an experiment that can probe the mass hierarchy [13]. The ICAL is most sensitive to atmospheric muon neutrinos (and antineutrinos), where the long tracks of muons produced in charged-current interactions of muon neutrinos (CC$\mu$) via $\nu_\mu N \to \mu^- X$ ($\bar{\nu}_\mu N \to \mu^+ X$) can be used to reconstruct both the magnitude and direction of their momenta, as well as the charge of the muon. Here, $X$ is any set of final-state hadrons. The advantage of having a magnetized iron calorimeter is its ability to clearly distinguish $\mu^+$ from $\mu^-$, which allows the differing matter effect for neutrinos and antineutrinos to be used to access the mass hierarchy. Hence, analyzing muon events will yield the bulk of the sensitivity to oscillation parameters. Several studies of atmospheric neutrino oscillation parameters using muon events at INO have been reported [14–17].

*aleenachacko@physics.iitm.ac.in
†indu@imsc.res.in
‡libby@iitm.ac.in
§behera@iitm.ac.in

 

Since neutrino experiments are statistically limited, any neutrino interactions that can be reconstructed in addition to the CC$\mu$ events in which there is at least one muon track can potentially improve the sensitivity to oscillation parameters. Here, we study the contribution from the subdominant electron-neutrino events, even though the detector configuration presents challenges in reconstructing the electron events correctly.

The ICAL will have sensitivity to atmospheric electron neutrinos (and antineutrinos) through the charged-current interaction (CC$e$), $\nu_e N \to eX$ ($\bar{\nu}_e N \to e^+ X$). So only the final-state electromagnetic and hadronic showers can be used to reconstruct the event. The passive elements between each sampling layer in the ICAL are iron plates of 5.6 cm thickness, which corresponds to approximately three radiation lengths, so the detector will have a limited capability to reconstruct the electromagnetic showers produced by the electrons. Previous simulation studies have characterized the sensitivity of ICAL to the hadron energy [18,19], and preliminary results are available [20] on its sensitivity to the hadron direction. Both the energy and direction are reconstructed through the pattern of hits that will be left by the hadronic shower in the detector. In this paper, for the first time, a detailed simulation study is made of the ability of the ICAL to reconstruct electrons and determine the $\nu_e$ momentum, and to examine the sensitivity of these events to neutrino-oscillation parameters. Such CC$e$ events appear as "trackless" events in the detector, in contrast to most CC$\mu$ events, where a final-state muon often produces a long track.

Note that there are other sources of trackless events, namely, neutral current (NC) events, where the final state lepton is not observed in the detector, as well as those CC$\mu$ events where the reconstruction algorithm for the muon track fails. In all these trackless events, only a shower is obtained; note, however, that for CC$e$/CC$\mu$ events, the shower includes hits from both electron/muon and the associated hadrons in the interaction, while for NC events, the shower is due to the hadrons alone. We analyze these trackless events and show that they have good sensitivity to the oscillation parameter $\theta_{23}$.

The rest of the paper is arranged in the following manner. We begin with the analysis of the pure CC$e$ sample in a hypothetical ICAL-like detector that is fully efficient and has perfect reconstruction of CC$e$ events. In Sec. II, we identify the regions in electron-neutrino energy and direction space, where there is sensitivity to the oscillation parameters. In Sec. III, we briefly describe the salient parts of the GEANT4 [21,22] ICAL detector code that are used in the analysis and also briefly discuss the generation of events in the detector using the NUANCE neutrino generator [23]. In Sec. IV, we perform a $\chi^2$ analysis to determine the sensitivity of CC$e$ events to the neutrino-oscillation parameters, assuming a hypothetical ICAL-like detector. In Sec. V, we consider the realistic case of sensitivity to oscillation parameters of the combined trackless sample of CC$e$, NC, and trackless CC$\mu$ events in the proposed ICAL detector at INO, including systematic uncertainties as well. We conclude with a discussion in Sec. VI.

## II. THE OSCILLATION PROBABILITIES

Detailed simulations studies indicating the potential of the ICAL to measure $\Delta m^2_{32}$ and $\theta_{23}$ have been performed using the dominant CC$\mu$ channel; these studies use reconstructed information about the muon momentum (magnitude and direction), the muon charge, and hadronic shower. Therefore, the contribution of CC$\mu$ events in determining the oscillation parameters is well understood. Here, we study the complementary set of events, where no track could be reconstructed in the event sample. These events include CC$e$ events, which have hitherto not been studied with the ICAL.

Figure 1 shows the relevant oscillation probabilities for CC$e$ events, $P_{ee}$ and $P_{\mu e}$, as a function of the zenith angle $\theta_\nu$ (direction of the neutrino with respect to the vertically upward direction) for a single value of neutrino energy ($E_\nu = 5$ GeV). Here, $P_{ee}$ is the survival probability of $\nu_e$, and $P_{\mu e}$ is the probability of conversion of $\nu_\mu$ to $\nu_e$ [24]. In the top panel of Fig. 1, $P_{ee}$ and $P_{\mu e}$, are shown for three different values of $\Delta m^2_{32}$, while the bottom panel shows their behavior for three different values of $\theta_{23}$. As can be seen from Fig. 1, the oscillation probability $P_{\mu e}$ is sensitive to both $\Delta m^2_{32}$ as well as $\theta_{23}$, while the survival probability $P_{ee}$ is sensitive to $\Delta m^2_{32}$ alone. In addition, the effect of the $\Delta m^2_{32}$ variation is opposite for both probabilities, *i.e.*, $P_{ee}$ increases with increasing $\Delta m^2_{32}$, $P_{\mu e}$ decreases with increasing $\Delta m^2_{32}$ and vice versa. The true values of the oscillation parameters used in this analysis are given in Table I, along with the $3\sigma$ confidence level (C.L.) for the parameters. We assume the normal ordering throughout this paper, unless otherwise stated, because trackless events have no sensitivity to mass ordering as $\nu$ and $\bar{\nu}$ are indistinguishable.

To see a significant oscillation signature in the distributions of electron events, either the survival probability $P_{ee}$ should be significantly less than 1 or the appearance probability $P_{\mu e}$ should be significantly greater than 0. Therefore, we explore the parameter sensitivity in the regions where $P_{ee} < 0.8$ and $P_{\mu e} > 0.1$ as a function of $\cos\theta_\nu$ and $E_\nu$ to establish whether there is enough sensitivity to proceed with further studies. Figure 2 shows $P_{ee}$ and $P_{\mu e}$ as a function of $E_\nu$ and $\cos\theta_\nu$. As expected, both $P_{\mu e}$ and $P_{ee}$ show potential sensitivity in the region where $E_\nu > 2$ GeV and $\cos\theta_\nu > 0$, which corresponds to upward-going neutrinos, with the highest sensitivity in the region around $E_\nu \sim 5$ GeV and $\cos\theta_\nu \sim 0.7$–$0.8$ ($\theta_\nu \sim 30°$–$45°$). The sensitivity of CC$\mu$ events to the oscillation parameters $\Delta m^2_{32}$ and $\theta_{23}$, via the dominant

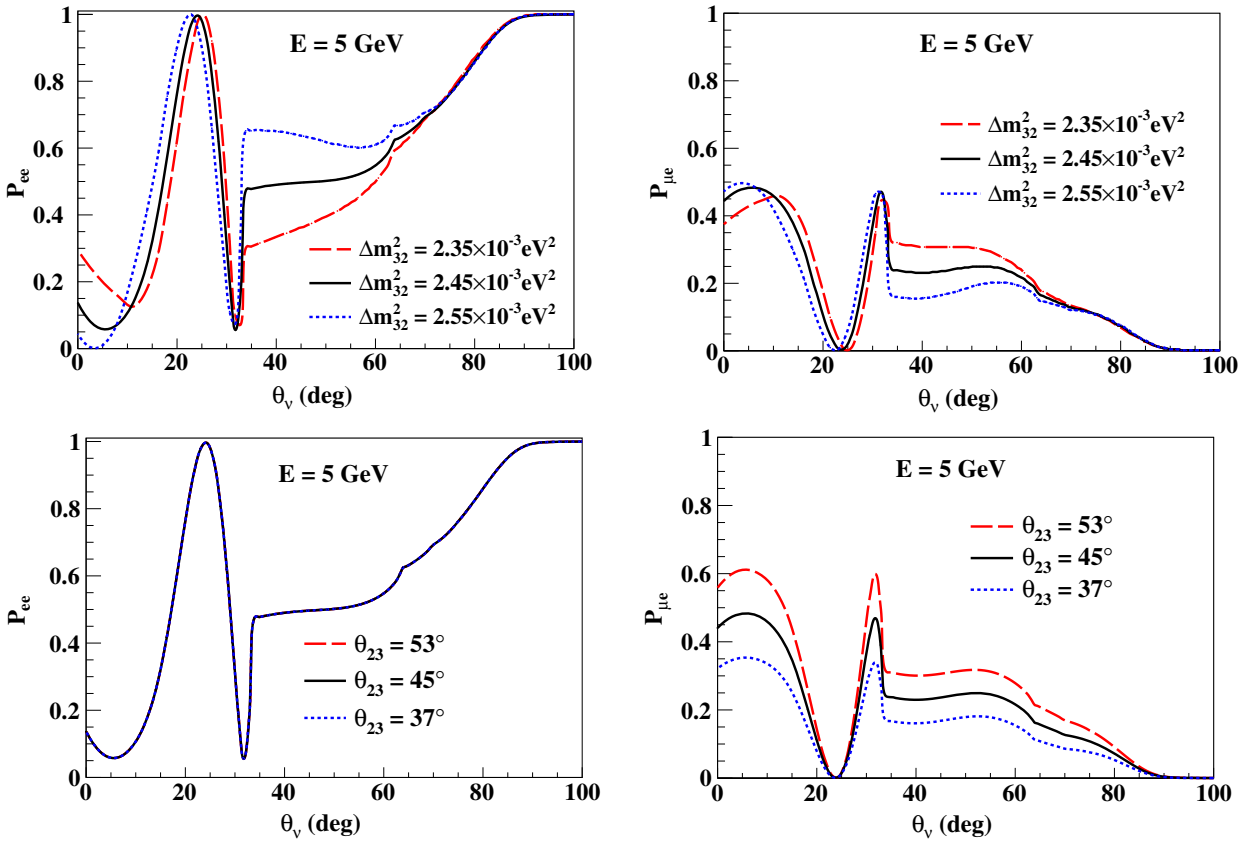


FIG. 1. $P_{ee}$ (top left) and $P_{\mu e}$ (top right) as a function of zenith angle, shown for three values of $\Delta m^2_{32}$ ($2.55 \times 10^{-3}$ eV$^2$ [dotted blue line], $2.45 \times 10^{-3}$ eV$^2$ [solid black line], $2.35 \times 10^{-3}$ eV$^2$ [dashed red line]). $P_{ee}$ (bottom left) and $P_{\mu e}$ (bottom right) as a function of zenith angle, shown for three values of $\theta_{23}$ [left] (53° [dashed red line], 45° [solid black line], 37° [dotted blue line]).

term proportional to $P_{\mu\mu}$, is well-understood and is not repeated here.

## III. EVENTS GENERATION AND ANALYSIS

Atmospheric neutrinos originate from the decay of particles in hadronic showers generated by cosmic rays, which are primarily composed of protons, interacting with the upper atmosphere. The hadronic showers contain many charged pions that subsequently decay almost exclusively via the following chain:

$$\pi^\pm \to \mu^\pm + \nu_\mu(\bar{\nu}_\mu); \qquad \mu^\pm \to e^\pm + \nu_e(\bar{\nu}_e) + \bar{\nu}_\mu(\nu_\mu).$$

It can be seen that the flux of muon neutrinos ($\Phi_\mu$) is approximately twice the electron-neutrino flux ($\Phi_e$), especially at low energies, where the muon subsequently decays before reaching the surface of the earth. These neutrinos interact with matter through CC and NC interactions.

TABLE I. Oscillation parameter values assumed for the analysis [25]. The values of $\sin^2\theta_{12}$, $\sin^2\theta_{13}$, and $\Delta m^2_{12}$ have been fixed at their central value, because marginalizing them over their present $3\sigma$ range causes very little change in the results.

| Parameter | Value | $3\sigma$ range |
|---|---|---|
| $\sin^2\theta_{12}$ | 0.307 | 0.268–0.346 |
| $\sin^2\theta_{23}$ | 0.51 | 0.39–0.63 |
| $\sin^2\theta_{13}$ | 0.0210 | 0.0177–0.0243 |
| $\Delta m^2_{21}$ [$10^{-5}$ eV$^2$] | 7.53 | 6.99–8.07 |
| $\Delta m^2_{32}$ [$10^{-3}$ eV$^2$] | 2.45 | 2.3–2.6 |
| $\delta_{CP}$ [deg] | 0 | 0–360 |

### A. Event generation with the NUANCE neutrino generator

Atmospheric neutrino interactions in the 50 kton ICAL detector for an exposure time of 100 years are simulated using the NUANCE neutrino generator, incorporating the Honda-3D atmospheric neutrino flux [26]. NUANCE generates these events for different cross sections, including quasielastic, resonance, and deep-inelastic scattering. Since generating NUANCE events for various oscillation parameters is quite time consuming, it is generated once for a specified detector exposure time, and the oscillation effects are later included event-by-event using the accept-or-reject method.

The number of events $N^P_\alpha(\alpha = e, \mu, \tau)$ that occur via the processes $P$, $P =$ CC, or NC, in a detector with $N_D$ targets during an exposure time $T$, is related to the product of the flux times the cross section. Therefore,

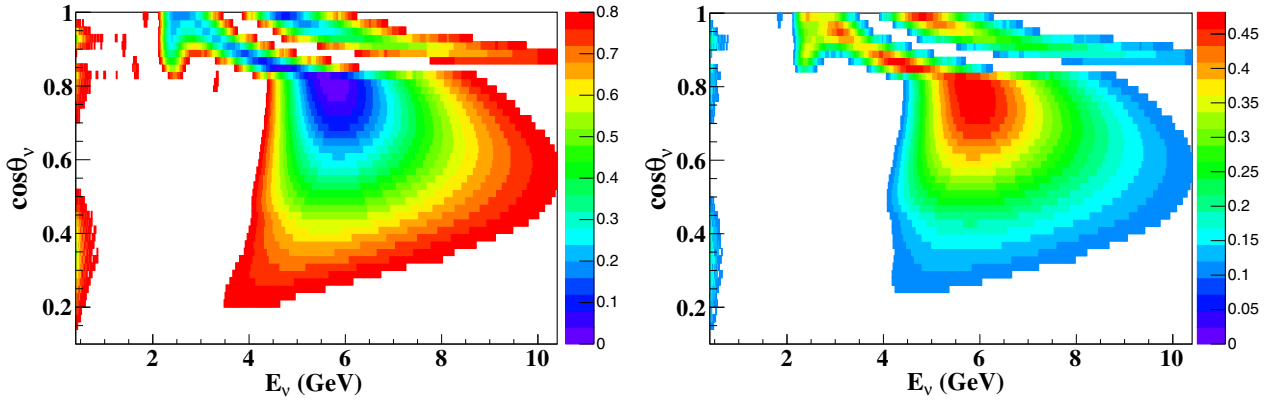


FIG. 2. $P_{ee} < 0.8$ (left) and $P_{\mu e} > 0.1$ (right) as a function of $E_\nu$ and $\cos\theta_\nu$.

$$N_\alpha^P = N_D \times T \int dE_\nu d\cos\theta_\nu \times \left[P_{e\alpha}\frac{d^2\Phi_e}{dE_\nu d\cos\theta_\nu} + P_{\mu\alpha}\frac{d^2\Phi_\mu}{dE_\nu d\cos\theta_\nu}\right]\sigma_\alpha^P(E_\nu), \quad (1)$$

where $\sigma_\alpha^P$ is the cross section for the interaction of neutrino flavor $\nu_\alpha$ via process $P$ in the detector. Here, $\Phi_e$ and $\Phi_\mu$ are the electron and muon atmospheric neutrino fluxes, respectively. A similar expression holds for antineutrinos as well.

In particular, $N_e^{\rm CC}$ and $N_\mu^{\rm CC}$ correspond to CC$e$ and CC$\mu$ interactions in ICAL. Note that

$$\sum_\alpha P_{\beta\alpha} = 1,$$

for $\beta = e, \mu$, the sum of all NC interactions,

$$N^{\rm NC} \equiv N_e^{\rm NC} + N_\mu^{\rm NC} + N_\tau^{\rm NC},$$

is independent of oscillation probabilities, thus the oscillation parameters. Therefore, only $N_e^{\rm CC}$ and $N_\mu^{\rm CC}$ are sensitive to the neutrino-oscillation parameters.

For the studies that simulate the ICAL, we need to reconstruct the events by a GEANT4-based detector simulation of the ICAL detector and furthermore, select the trackless events in this sample. We discuss how to achieve this in the next section. However, we point out in advance that the inelasticity distribution of all these classes of events is found to be similar, as can be seen from Fig. 3. Here, the inelasticity parameter is $y = 1 - E_{\rm lepton}/E_\nu$, where the final state lepton could be a charged or a neutral lepton for CC/NC events. This is important for the analysis since a difference in the inelasticities of the different classes of events can differentially alter the energy dependence of the relevant cross sections. This could in turn skew the event rates differently and affect the analysis substantially.[1]

[1]We thank the referee for pointing out this.

### B. Event generation with GEANT

A major part of the INO proposal is the construction of a 50 kton magnetized ICAL [27]. The ICAL will be built in three modules each with a size of 16 m × 16 m × 14.5 m (length × width × height). Each module will comprise of 151 layers of 5.6 cm thick iron plates, which will be magnetized to a strength of about 1.5 T using copper coils. The active detector elements of the ICAL will be the resistive plate chambers (RPCs) [27]. The RPCs are gaseous detectors constructed by placing 2 mm spacers between two 3 mm thick glass plates of area 2 m × 2 m and are operated at a high voltage of 10 kV in avalanche mode. Each of these RPCs will be interleaved into the 4 cm gap between the iron layers. The detector will be sensitive to muons and other charged particles produced in the interactions of atmospheric neutrinos with the iron nuclei. This geometry and magnetic field have been coded into

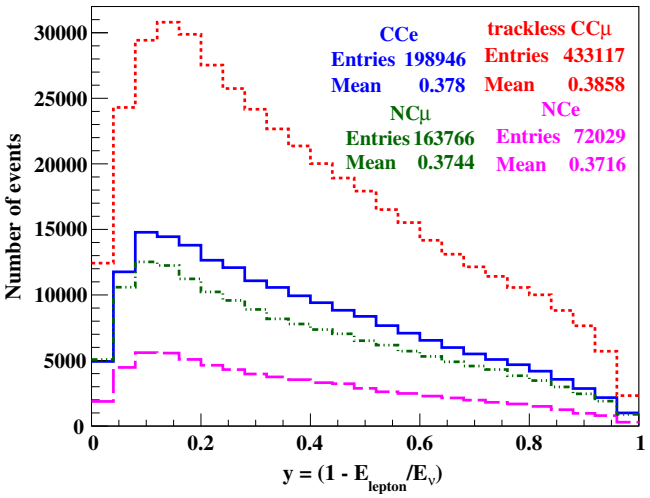


FIG. 3. Distributions of various classes of "trackless" events —CC$e$ (solid blue line), NC$e$ (dashed pink line), NC$\mu$ (dot-dashed green line), and CC$\mu$ events for which the reconstruction algorithm failed to reconstruct a track (dotted red line)—as a function of the inelasticity parameter, $y$.

a GEANT4-based simulation of the detector response. The RPCs are considered to have a timing resolution of 1 ns, which is important to distinguish up-going from down-going events.

The dominant signals from atmospheric neutrinos in the ICAL detector are from CC$\mu$ events. The CC$e$ events form the subdominant signal, both due to smaller fluxes and also because ICAL is optimized for detecting CC$\mu$ events. We also have NC interactions, but the cross section for these interactions are small compared to CC$\mu$ interactions [28].

The NUANCE-generated events are passed through the GEANT4-based simulation of the ICAL detector. Each event leaves a pattern of hits in the sensitive RPC detector. Long tracklike events are typically associated with the minimum-ionizing muons. Using information about the local magnetic field that is incorporated into the GEANT code, a Kalman-filter algorithm [29] is used to identify and reconstruct possible "tracks," which can be fitted to yield the particle momentum and sign of charge. Events where no track could be reconstructed are identified as *trackless events*. Notice that events which pass through less than four layers of the detector are not sent to the Kalman filter for track reconstruction and hence, are included in the trackless events sample.

In order to analyze these events, we need to calibrate the hits to the energy and direction associated with each event. We first consider the CC$e$ events alone.

### C. Direction reconstruction of trackless events

To reconstruct the direction of the shower, we use a method referred to as the *raw-hit method* [20]. A charged particle, produced by the interaction of neutrinos with the detector, while passing through an RPC, produces induced electrical signals. These signals are collected by copper pick-up strips of width 2 cm, which are placed orthogonal to each other on either side of the RPC. The center of the pickup strips defines $x$ or $y$ coordinate of the hits, and the center of the RPC air-gap defines the $z$ coordinate. The signals in the copper strips thus provide either $(x, z)$ or $(y, z)$ information and are considered as "hits," which are used to reconstruct the average energy and direction of the shower. Due to the coarse position resolution of the ICAL detector, it is difficult to distinguish between electron and hadron showers. Since in CC$e$ and trackless CC$\mu$ events, the shower actually arises from both the electron/muon and hadrons in the final state, the net reconstructed direction will point back to that of the original neutrino, especially at higher energies since the final state particles from such events are forward peaked. This is in contrast to the direction reconstruction of showers in CC$\mu$ events, where the muon track is reconstructed; here, the direction of the shower determines the net direction of the hadrons alone, since the direction of the muons can be independently determined. Finally, since the final state lepton is not detected in NC events, the shower direction is that of the hadrons in the event, just as in the case of CC$\mu$ events with a reconstructed track.

If two or more $x$ and $y$ strips have signals within a single RPC in an event, there is an ambiguity in the definition of the $(x, y)$ hit position. One or more of the positions are fake and are referred to as a *ghost hit*. Therefore, the reconstruction is done separately in the $x$-$z$ and $y$-$z$ planes to avoid these ghost hits. Since the electron or hadron showers are insensitive to the magnetic field, the average direction of the shower is reconstructed as

$$\theta_{\rm reco} = \tan^{-1}\sqrt{m_x^2 + m_y^2}; \qquad \phi = \tan^{-1}\left(\frac{m_y}{m_x}\right), \quad (2)$$

where $m_{x[y]}$ are the slopes of straight line fits to the $(x, z)$ $[(y, z)]$ hit positions. The simulation requires that the hits are within a timing window of 50 ns to ensure they are only from the event under consideration. Requirements on the minimum number of layers with hits ($\geq$2) and minimum number of hits per event $n_{\rm hits}$ ($\geq$3) are applied at the reconstruction level to ensure that there are sufficient hits passing through enough layers to fit a straight line. Around 46% of the events satisfy these criteria. The time information from each of these hit distributions, *i.e.*, the slopes of the $t_x$ vs $z$ and $t_y$ vs $z$ distributions, allows us to reconstruct whether the event is an up-going or down-going one. Approximately 10% of events have time slopes from the $t_x$-$z$ and $t_y$-$z$ distributions of opposite signs; these events are discarded. Figure 4 shows an example of an up-going CC$e$ event and the corresponding position of hits in that event in the $x$-$z$ and $y$-$z$ planes.

Figure 5 shows the migration matrix for the reconstructed direction $\cos\theta_{\rm reco}$ as a function of the true direction $\cos\theta_\nu$, for CC$e$ events. As expected, the reconstruction is poor in the horizontal direction, i.e., $-0.2 \leq \cos\theta_\nu \leq 0.2$, and improves towards the vertical, although some fraction of the events are reconstructed in the wrong quadrant (with $\theta_{\rm reco} \sim \pi - \theta_\nu$).

The reconstruction efficiency $\epsilon_{\rm reco}$ and relative directional efficiency $\epsilon_{\rm dir}$ are given by

$$\epsilon_{\rm reco} = \frac{N_{\rm reco}}{N}, \qquad \epsilon_{\rm dir} = \frac{N'_{\rm reco}}{N_{\rm reco}}, \quad (3)$$

where $N_{\rm reco}$ is the number of events reconstructed from the total number of events ($N$), and $N'_{\rm reco}$ is the number of the events correctly reconstructed as up going or down going. Figure 6 shows $\epsilon_{\rm reco}$ and $\epsilon_{\rm dir}$ as functions of $\cos\theta_\nu$ for CC$e$ events. The $E_\nu$ and $\cos\theta_\nu$ averaged values of $\epsilon_{\rm reco}$ and $\epsilon_{\rm dir}$ are $(41.7 \pm 0.2)\%$ and $(66.8 \pm 0.2)\%$, respectively, showing that we can indeed distinguish the up-going events from the down-going events, which is crucial for the oscillation studies.

Figure 7 (left panel) shows the $\cos\theta_\nu$ distribution before and after reconstruction for CC$e$ events. Notice that angular

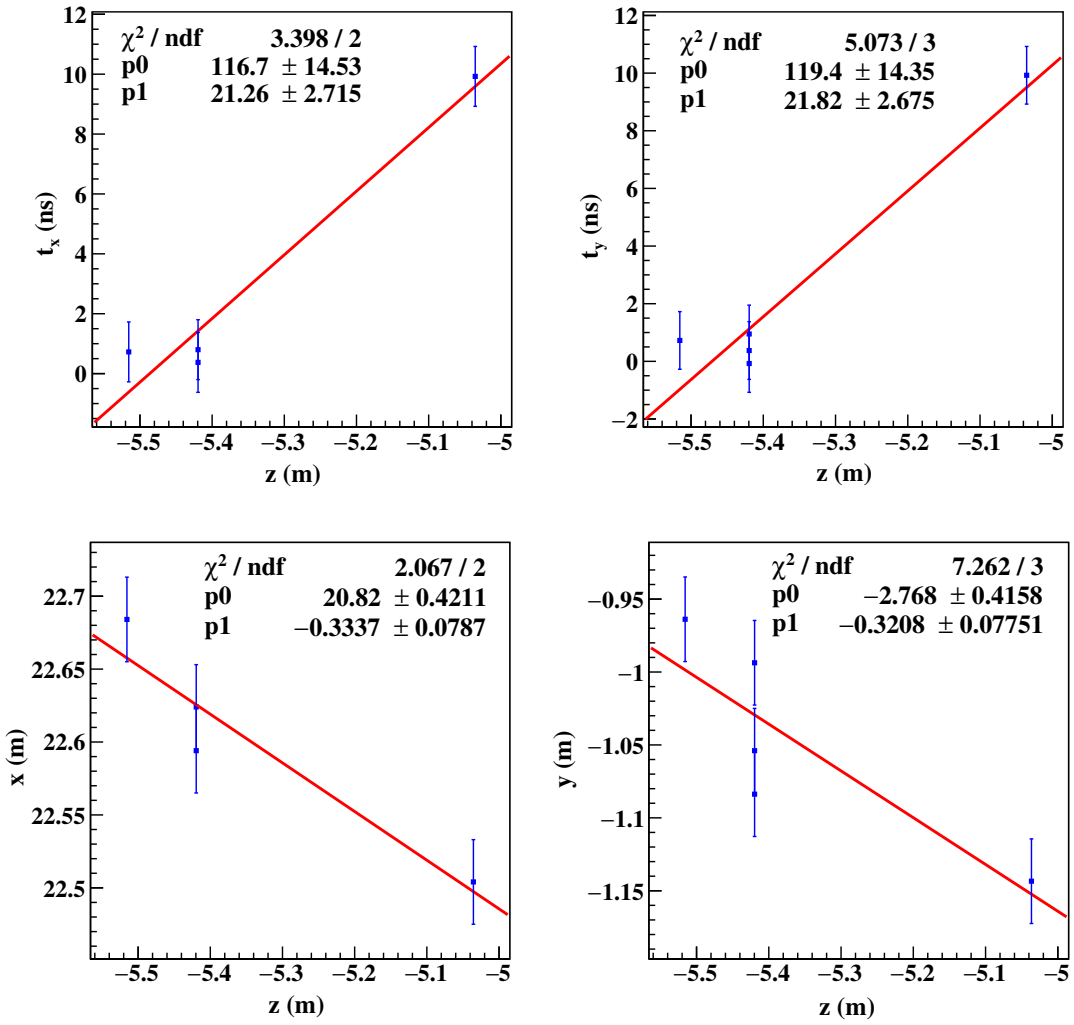


FIG. 4. Example fits (top panel) to $z$ vs $t_x$ (left) and $z$ vs $t_y$ (right) distributions for one event which was produced by an electron neutrino with $E_\nu = 1.59$ GeV and $\cos\theta_\nu = 0.48$. Fits to the distribution (bottom panel) of $z$-$x$ (left) and $z$-$y$ (right) hits for the same example event. Here, $p0$ and $p1$ are the intercept and slope of the fit, respectively.

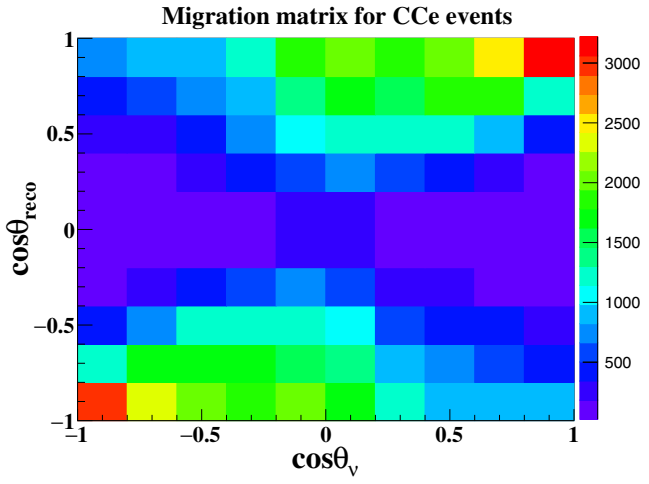


FIG. 5. Reconstructed direction $\cos\theta_{\rm reco}$ as a function of the true direction $\cos\theta_\nu$ for CC$e$ events.

smearing leads to an excess of events in the vertical directions compared to the NUANCE level events while leaving very few events in the horizontal bins.

The NC and trackless CC$\mu$ events are reconstructed and analyzed similar to the CC$e$ events. It turns out that the fraction of CC$\mu$ events for which no track was reconstructed is substantial, about 53% of the total CC$\mu$ events, which occurs because of the large fluxes at low energies. The primary reason why the Kalman filter algorithm fails to fit a track for these cases is because of the small number of hits in these events; we discuss this further when we consider energy reconstruction below.

It can be seen from Fig. 8 that the direction reconstruction is best (worst) for CC$\mu$ (NC) events, as expected. The distribution of these events is shown in the right-hand panel of Fig. 7, and the reconstruction efficiency for all classes of trackless events is shown in Fig. 9.

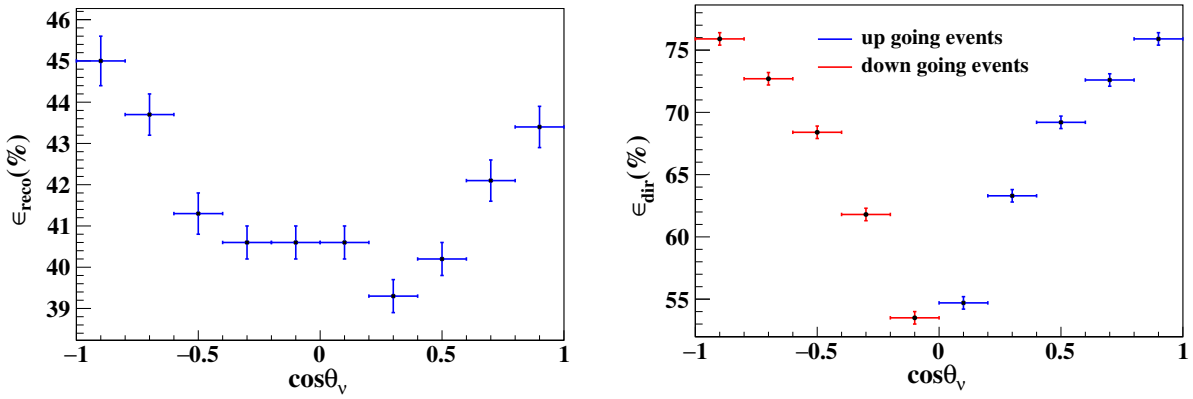


FIG. 6. Reconstruction efficiency, $\epsilon_{\text{reco}}$ (left) and the relative directional efficiency $\epsilon_{\text{dir}}$ (right) as a function of $\cos\theta_\nu$ for CC$e$ events. Note that the $y$-axis scales on the two graphs are different.

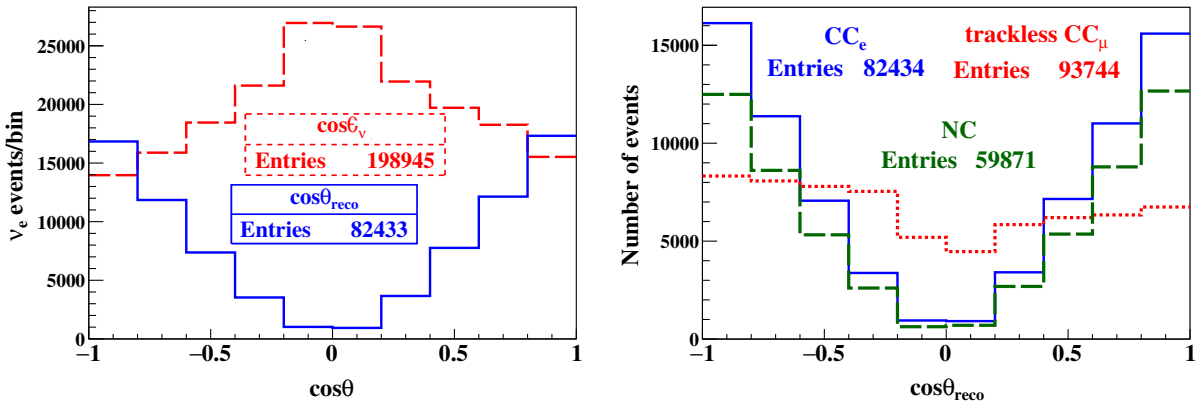


FIG. 7. Left: The distribution of the $\cos\theta_\nu$ (dashed red line) and reconstructed $\cos\theta_{\text{reco}}$ (solid blue line) for an exposure of 100 years, assuming a 50 kton detector. Right: $\cos\theta_{\text{reco}}$ CC$e$ (blue solid), trackless CC$\mu$ (red dotted), and total NC (green dashed lines) events.

### D. Energy reconstruction of trackless events

The total energy reconstructed from the hit information is labeled as $E_{\text{reco}}$. As discussed above, for the CC$e$ and CC$\mu$ events sample, this should give the incident neutrino energy, whereas for NC events, this is the hadron energy in the final state. It is not possible to obtain the reconstructed energy directly from the hit information; rather, it is inferred via a calibration of the number of hits as a function of the true energy. Taking into consideration the same selection criteria applied for direction reconstruction, we remove three hits from each event so that we calibrate true energy vs $(n_{\text{hits}} - 3)$. Distributions of hits in distinct energy ranges are formed. Figure 10 (left) shows an example of hits distribution in the energy range 5.9 to 6.4 GeV for CC$e$ events. For each of these hit distributions, the mean of number hits $\bar{n}(E)$ is plotted against the mean energy $\bar{E}$ of events within a specific energy range. These data are then fit to

$$\bar{n}(E) = n_0 - n_1 \exp(-\bar{E}/E_0), \tag{4}$$

where $n_0$, $n_1$ and $E_0$ are constants, as shown in the right side of Fig. 10.

#### 1. Reconstructing the energy from the number of hits

After obtaining the values of the constants $n_0$, $n_1$ and $E_0$, we invert Eq. (4) to estimate the reconstructed energy, $E_{\text{reco}}$.

It can be seen from Fig. 10 that every energy bin corresponds to a range in *nhits*, with a different mean and rms. To obtain the reconstructed energy for the analysis from the *nhits* of that event, an inversion is required. For each event, the *nhits* of that event was assumed to be the mean value from which a "mean" reconstructed energy was found, from the right-hand figure in Fig. 10. This value was then smeared depending on the rms of the histogram corresponding to the energy bin to which the reconstructed energy belongs. The energy obtained by thus incorporating the finite detector resolution was considered to be the reconstructed energy $E_{\text{reco}}$ of the event.

The migration matrix showing the correspondence between true and reconstructed energy is shown in

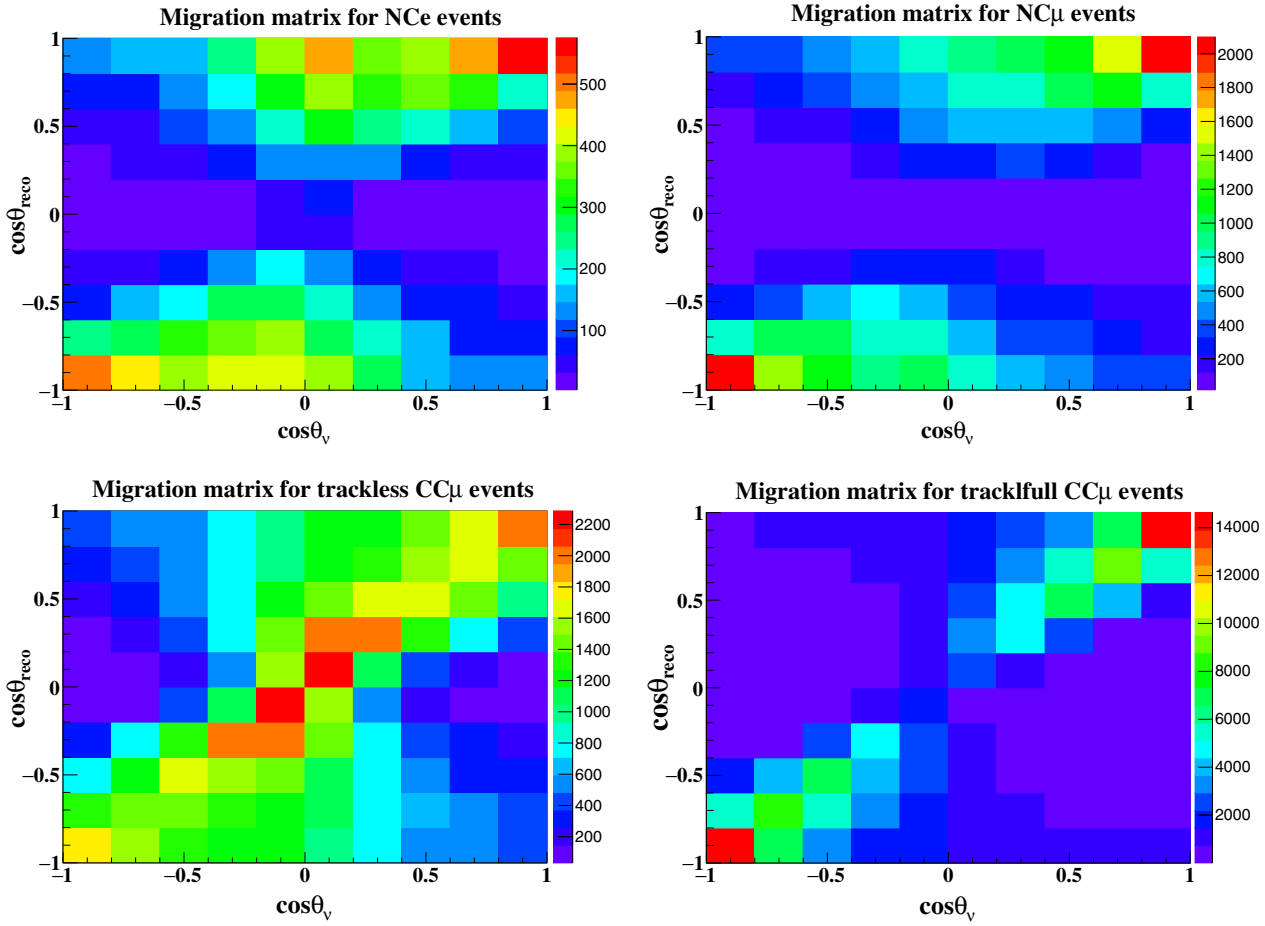


FIG. 8. Reconstructed direction $\cos\theta_{\text{reco}}$ as a function of the true direction $\cos\theta_{\nu}$ for NC$e$ events (top left), NC$\mu$ events (top right), CC$\mu$ events without reconstructed tracks (bottom left), and CC$\mu$ events with at least one track reconstructed by a Kalman filter algorithm (bottom right).

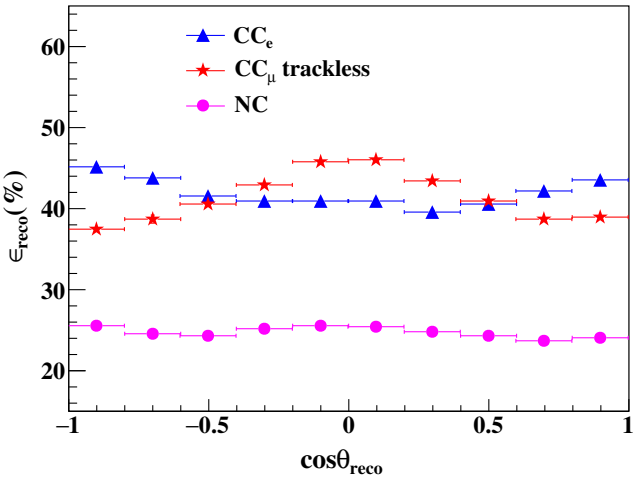


FIG. 9. Reconstruction efficiency as a function of direction ($\cos\theta_{\text{reco}}$) for CC$e$ (blue triangle), trackless CC$\mu$ (red star), and NC (pink circle) events that comprise the total sample of trackless events.

Fig. 11. We see that the reconstructed events have shifted towards higher energy. A significant fraction of the lower energy events are reconstructed as higher energy events because of the upper tail in $n_{\text{hits}}$ distribution (see Fig. 10), because of which we have more reconstructed events with higher energy. The effect of this on the reconstructed spectrum can be seen in Fig. 12, which shows the energy distribution for CC$e$ events before and after reconstruction.

It can also be seen from Fig. 11 that the class of CC$\mu$ events with no reconstructed track ("trackless CC$\mu$ events") has the lowest energy distribution, both before and after reconstruction, clearly indicating that the Kalman filter for track recognition failed for these events because of the small number of hits generated due to their low energies, as can be seen from Fig. 13. We now use these samples of reconstructed events and analyze their sensitivity to various neutrino oscillation parameters, in particular, to $\sin^2\theta_{23}$.

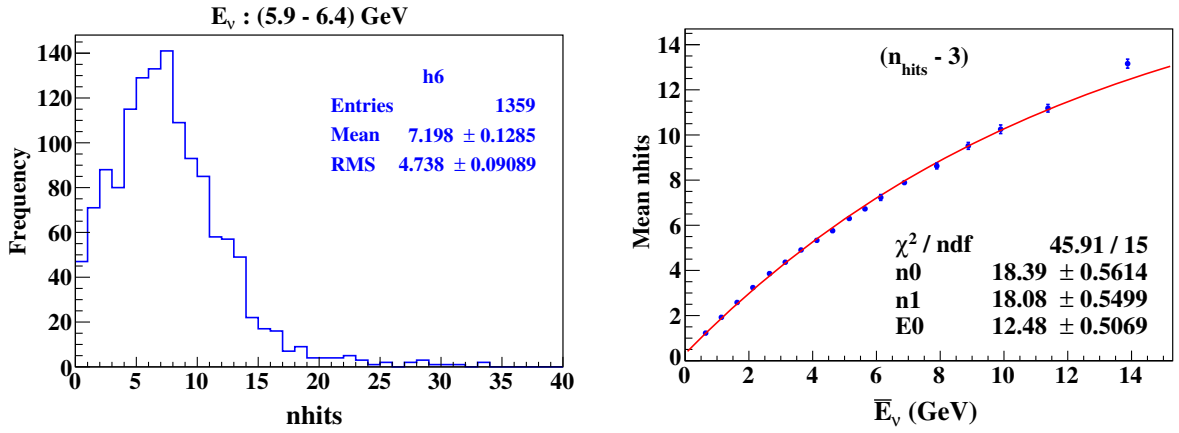


FIG. 10. Left: example of hits distribution in the $E_\nu$ range (5.9 to 6.4) GeV. Right: $\bar{n}(E)$ vs $\bar{E}$ with the fit superimposed.

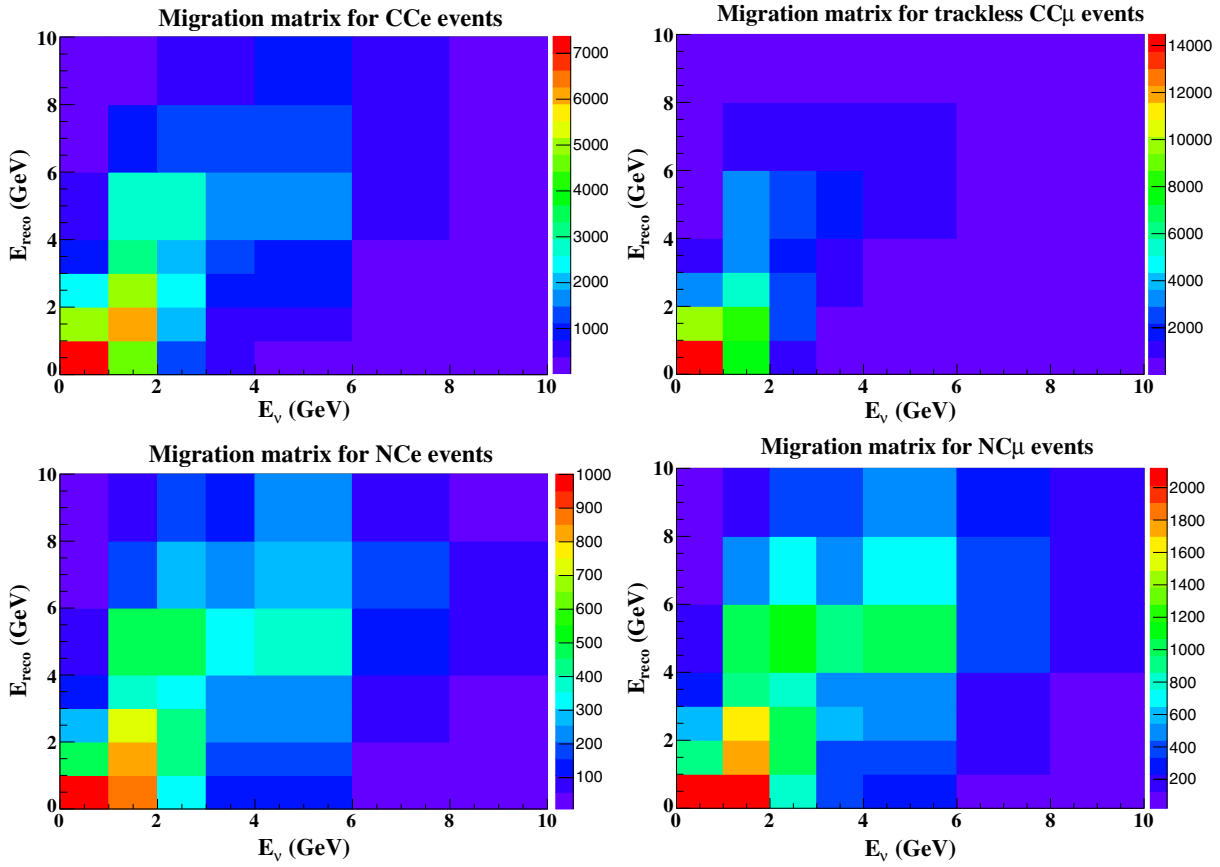


FIG. 11. Reconstructed energy $E_{\text{reco}}$ as a function of true energy $E_\nu$ for all classes of trackless events.

## IV. SENSITIVITY OF ELECTRON EVENTS TO OSCILLATION PARAMETERS

### A. Analysis of pure CC$e$ events

To understand the potential sensitivity to $\sin^2\theta_{23}$ we start by performing a study of pure CC$e$ events, assuming a hypothetical ICAL-like detector with 100% reconstruction efficiency and perfect resolution. This provides a benchmark for the maximum amount of information regarding neutrino oscillations that can be extracted from the ICAL data.

The following simulation algorithm is used to incorporate oscillations for CC$e$ events. The CC$e$ events have contributions from the $\nu_e$ fluxes via the first term in Eq. (1), *viz.*, $\Phi_e\sigma_e^{CC}$, weighted by $P_{ee}$, and similarly, from the $\nu_\mu$

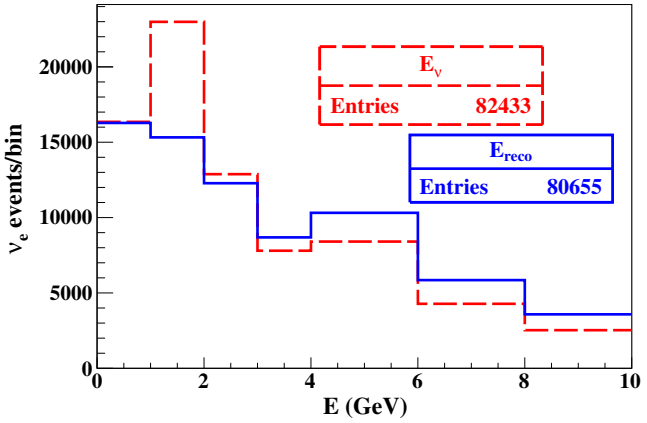


FIG. 12. Distribution of true $E_\nu$ (dashed red lines) and reconstructed $E_{\text{reco}}$ (solid blue lines) energy for CC$e$ events for an exposure of 100 years assuming a 50 kton detector.

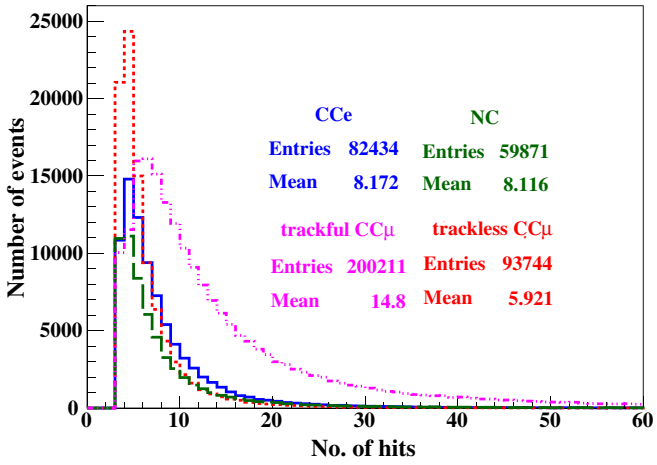


FIG. 13. Distribution of hits for CC$e$ (solid blue), NC (dashed green), CC$\mu$ with at least one reconstructed track (dot-dashed pink) and trackless CC$\mu$ (dotted red line).

flux via the second term. The weight is implemented as follows. A uniform random number $r$ between 0 and 1 is generated. Those events for which $P_{ee} > r$ are taken to be survived electron events. Similarly, NUANCE events are generated in which the electron and muon fluxes are swapped. This corresponds to events from the second term, *viz.*, $\Phi_\mu \sigma_e^{CC}$, weighted by $P_{\mu e}$. Then the oscillation probability $P_{\mu e}$ is calculated for every swapped $\nu_e$ event; see Eq. (1). Those events for which $P_{\mu e} > r'$, where $r'$ is a uniform random number between 0 and 1, are taken to be oscillated electron events. Figure 14 shows the fraction of CC$e$ events arising from survived and oscillated fluxes at the NUANCE generator level, for a sample of ten years of data.

Approximately 94% of $\nu_e$ events survive, while only ~3% of $\nu_\mu$ events oscillate into $\nu_e$ due to the smallness of $\theta_{13}$. However, note that these events are direction dependent; in addition, they arise from a term containing the atmospheric *muon neutrino* fluxes, as can be seen from Eq. (1), which are roughly twice the electron neutrino fluxes; hence, the contribution of these events, roughly 6% of the total electron neutrino events, will turn out to be significant.

Figure 15 shows the ratio of oscillated to unoscillated events of the total (survived and oscillated) electron events, again, at the NUANCE generator level. The oscillation signature is most prominent for up-going neutrinos ($\cos\theta > 0.5$) with $E_\nu \sim 2$–7 GeV.

### B. Sensitivity after reconstruction

Using the simulation algorithm the oscillations were again incorporated in the unoscillated flux of reconstructed $\theta_{\text{reco}}$ and $E_{\text{reco}}$. Figure 16 shows the ratio of oscillated to unoscillated $\cos\theta_{\text{reco}}$ and $E_{\text{reco}}$ distributions for selected CC$e$ events. As seen when comparing with Fig. 15, where we had taken a sample corresponding to ten years of data,

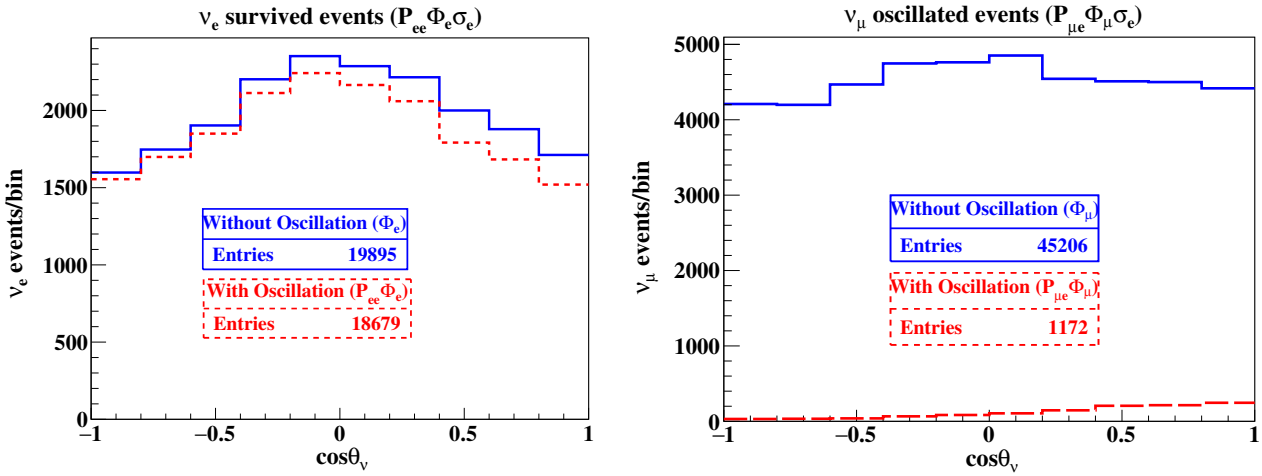


FIG. 14. Simulated $\cos\theta$ distributions for CC$e$ events arising from ten years exposure from survived $\nu_e$ (left) and oscillated $\nu_\mu$ events (right), with (solid blue line) and without (dashed red line) including oscillation probabilities $P_{\alpha e}$, implemented at the NUANCE level.

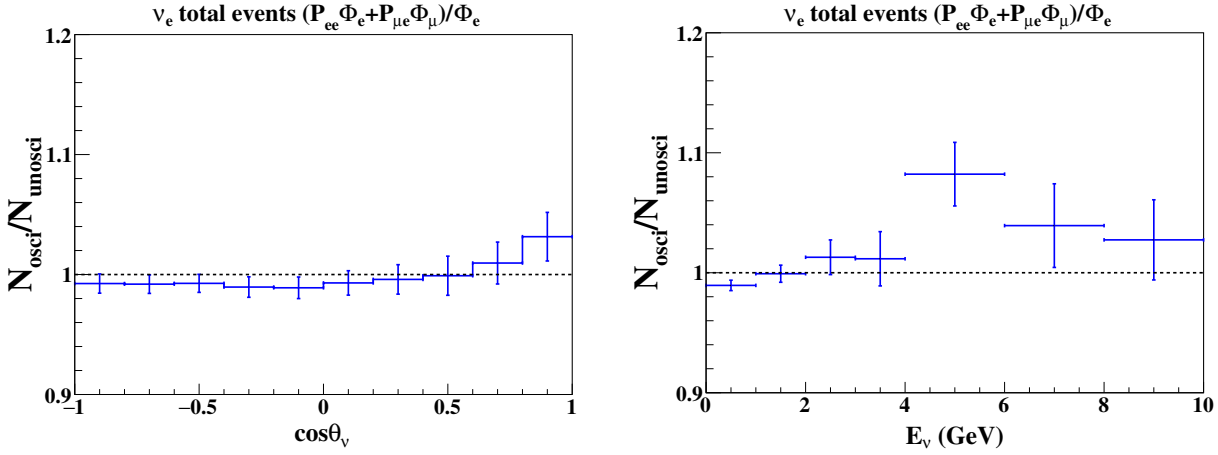


FIG. 15. Ratio of oscillated to unoscillated CC$e$ NUANCE-generated events as a function of $\cos\theta_\nu$ (left) and $E_\nu$ (right), corresponding to ten years of data, assuming a 50 kton detector.

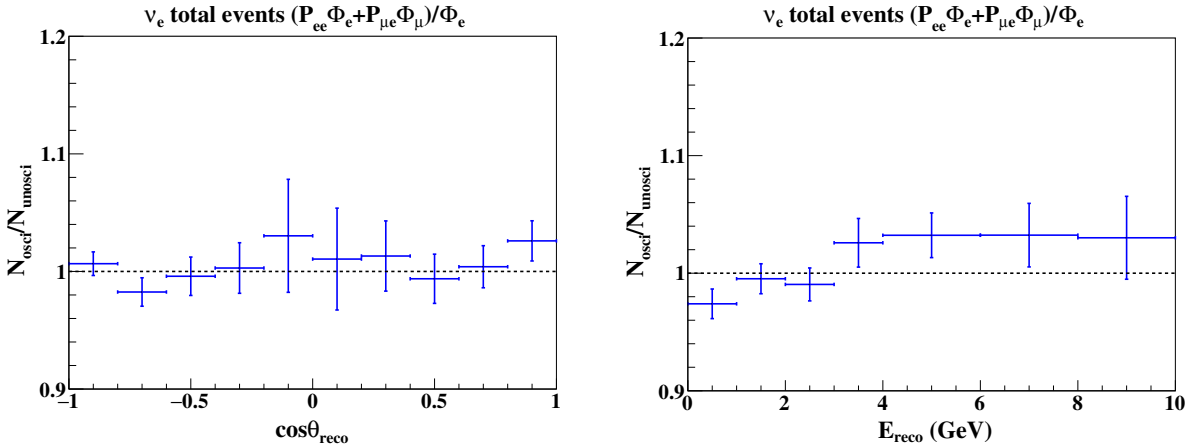


FIG. 16. Ratio of GEANT-reconstructed oscillated to unoscillated CC$e$ events as a function of $\cos\theta_{\rm reco}$ (left) and $E_{\rm reco}$ (right), for an exposure of ten years, assuming a 50 kton detector.

assuming 100% efficiency and perfect resolution, even after reconstruction the oscillation signature is still prominent in regions where $E_\nu > 2$ GeV and $\cos\theta_\nu > 0.5$.

To assess the sensitivity of pure CC$e$ events in ICAL to oscillation parameters, a $\chi^2$ analysis is performed assuming an ICAL-like detector that can also perfectly reconstruct and discriminate such pure CC$e$ events; the analysis, including all trackless events, is presented in the next section. First, the simulated data, scaled to ten years, oscillated with the true values of the oscillation parameters as given in Table I, are labeled as being the "observed data" and binned in ten $\cos\theta_{\rm reco}$ bins of equal width and seven $E_{\rm reco}$ bins of unequal width in the range 0 to 10 GeV (see Fig. 16) for the statistical analysis. The theoretical fits to these data are provided by scaling down the 100 years simulated data to ten years using a set of oscillation parameters varied in their $3\sigma$ ranges. The fit is the minimization of a Poissonian $\chi^2$,

$$\chi^2 = 2\sum_i \sum_j \left[ (T_{ij} - D_{ij}) - D_{ij} \ln\left(\frac{T_{ij}}{D_{ij}}\right)\right], \qquad (5)$$

where $T_{ij}$ and $D_{ij}$ are the "theoretically expected" and "observed number" of events respectively, in the $i^{\rm th}$ $\cos\theta_{\rm reco}$ bin and $j^{\rm th}$ $E_{\rm reco}$ bin. We find that this hypothetical case with a sample of just CC$e$ events, without including other trackless events and systematic uncertainties, does show sensitivity to neutrino oscillation parameters.

Figure 17 shows the effect of binning in $\cos\theta_{\rm reco}$ and $E_{\rm reco}$ separately, as well as binning in both observables. With binning in $\cos\theta_{\rm reco}$ alone, we find that it is possible to obtain a relative $1\sigma$ precision[2] on $\sin^2\theta_{23}$ of 20%. There is no significant change when the events are binned in both

[2]Relative $1\sigma$ precision is defined as $1/4^{\rm th}$ of the $\pm 2\sigma$ variation around the true value of the parameter [13].

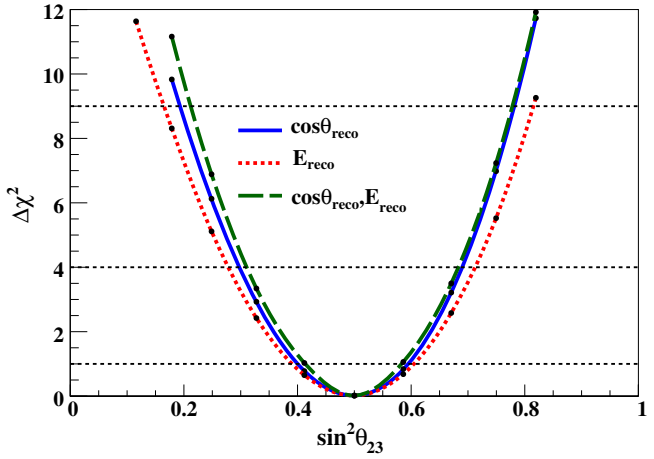


FIG. 17. $\Delta\chi^2$ as a function of $\sin^2\theta_{23}$ with bins in $\cos\theta_{\rm reco}$ (solid blue lines) alone, $E_{\rm reco}$ (dotted red lines) alone and in both (dashed green lines) $\cos\theta_{\rm reco}$ and $E_{\rm reco}$, for an exposure of ten years, assuming a 50 kton detector. "Data" were generated with true $\sin^2\theta_{23} = 0.5$.

observables. Therefore, for the rest of the analysis, we present results from fits to $\cos\theta_{\rm reco}$ bins alone, with events summed over all $E_\nu$. Since the effect of increasing (decreasing) $\Delta m^2_{32}$ leads to an increase (decrease) and decrease (increase) in $P_{ee}$ and $P_{\mu e}$, respectively (Fig. 1 top panel), sensitivity to $\Delta m^2_{32}$ from CC$e$ events in ICAL is inconsequential. Hence, in the rest of the paper, we consider the sensitivity to $\theta_{23}$ alone. We now consider a realistic analysis of all trackless events.

## V. REALISTIC ANALYSIS OF TRACKLESS EVENTS IN ICAL

### A. Selection criteria

Since the CC$e$ events have been reconstructed through their showers (both electromagnetic and hadronic), the NC events that produce showers (only hadronic) may be misidentified as CC$e$ events, even though we expect the shower pattern to be different in these two cases. We have already shown in Fig. 3 that the inelasticity parameter $y$ cannot be used to separate the different event classes. A useful set of parameters to separate these events is the number of layers ($l$) that the shower has traversed and the average hits per layer ($s/l$) in an event, $s$ being the number of hits in that layer [30]. While both CC$e$ and NC events are expected to traverse fewer layers than CC$\mu$ events (since the muon is a minimum-ionizing particle that leaves long "tracks" in the detector), it is expected that CC$e$ events will have larger $s/l$ because of the nature of the events. In addition, sometimes, due to large scattering or low energies giving a small number of hits, the Kalman-filter algorithm fails to reconstruct even a single track for CC$\mu$ events. Hence, such "trackless" events also have showers as their signatures in the detector and can also be misidentified as CC$e$ or NC events. In a realistic analysis with a detector such as ICAL, all these events need to be considered together.

Samples of CC$\mu$ events are generated from the NUANCE neutrino generator using the same algorithm as for CC$e$ events. Again, the "swapped events" in this case are also small due to the smallness of $P_{e\mu}$. Those events where the Kalman filter algorithm fails to reconstruct a track are collected together as "trackless CC$\mu$ events." Finally, samples of NC events are generated in the same way and are independent of the oscillation probabilities, $P_{\beta\alpha}$.

The CC$\mu$ events have very small $s/l \sim 1.5$ due to the minimum-ionizing nature of muons, as can be seen in Fig. 18. It can be seen that requiring $s/l > 2$ increases the purity of CC$e$ events, but it decreases the number of events in the sample, especially since a large fraction of CC$e$ events correspond to low energies and hence, traverse fewer layers. Here, efficiency is defined as the percentage of CC$e$ events passing the $s/l$ selection in total CC$e$ events, and purity is the percentage of CC$e$ events in all type of events passing $s/l$ selection.

Different selection criteria on $s/l$, $s/l > 1$, $s/l > 1.4$, $s/l > 1.8$, and $s/l > 2$, were used and the sensitivity to $\sin^2\theta_{23}$ determined. It was found that the sensitivity is dominated by the statistics, since the harder cuts decrease the total number of events available in the analysis. While efforts are ongoing to improve the Kalman-filter algorithm, as well as to improve the efficiency of separating the CC$e$ from the NC and trackless CC$\mu$ events, in what follows, we include all events (CC$e$, NC, and trackless CC$\mu$) in the analysis and do not apply any further selection criteria on $s/l$.

In the next section of this paper, we examine the effect of the inclusion of all these trackless events on the sensitivities to the neutrino-oscillation parameters.

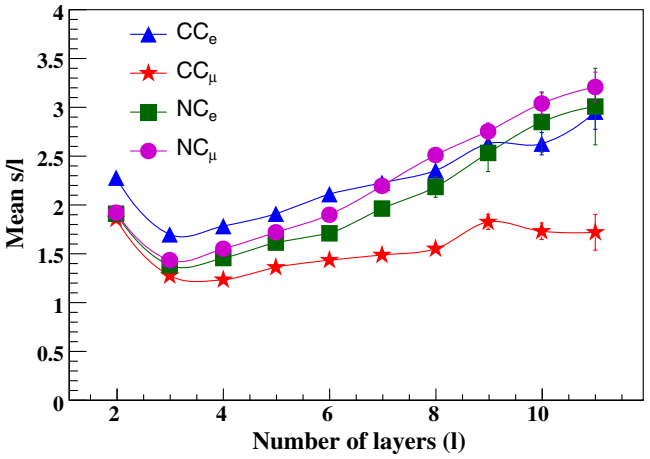


FIG. 18. Mean of average hits per layer($s/l$) as a function of number of layers($l$) for CC$e$ (blue triangle), trackless CC$\mu$ (red star), and NC (pink circle for NC$e$ and green square for NC$\mu$) events.

### B. $\chi^2$ analysis of the entire sample of trackless events

We now repeat the $\chi^2$ analysis, including all trackless events. As before, the parameters not being studied are fixed at their true values as given in Table I. Since $\theta_{13}$ is so precisely known, it is also kept fixed in the analysis. We consider the inclusion of systematic errors in the next section.

With the inclusion of all trackless events, the Poissonian $\chi^2$ without systematics is

$$\chi^2 = 2\sum_i \left[ T_i - D_i - D_i \ln\left(\frac{T_i}{D_i}\right)\right], \tag{6}$$

where $T_i$ now include the original CC$e$ events, and both the NC and trackless CC$\mu$ events as well, in the $i^{\text{th}}$ $\cos\theta_{\text{reco}}$ bin. The result of the analysis for the sensitivity to $\sin^2\theta_{23}$ is shown in Fig. 19. It can be seen that inclusion of all trackless events increases the relative $1\sigma$ precision on $\sin^2\theta_{23}$ to 15%. The improvement in sensitivity to $\sin^2\theta_{23}$ can be understood as the effect of inclusion of the low energy trackless CC$\mu$ events (∼42% of total CC$\mu$ events), since NC events do not have sensitivity to oscillation parameters and simply improve the overall normalization uncertainties. In addition, the result is mildly sensitive to the number of $\cos\theta_{\text{reco}}$ bins, especially in the first octant; this is true for the pure CC$e$ analysis as well.

### C. Including systematic uncertainties

So far, we have not considered the effect of systematic uncertainties on the sensitivities. We incorporate them through the pull method [31,32], where each independent source of systematic uncertainty is added to the difference of the theoretically expected and observed events through an univariate Gaussian random variable ($\xi$) referred to as the *pull*. To avoid overestimation of the systematic uncertainties, penalties are implemented by adding $\xi^2$ terms. We consider two sources of systematic uncertainties: ($i$) a 5% uncertainty on the flux dependency on $\theta_\nu$ [31] and ($ii$) a 2% uncertainty on the efficiency of reconstruction. In principle, it is possible to include an additional systematic uncertainty due to the overall flux normalization; however, a detailed analysis of the higher energy ($E_\nu > 1$ GeV) CC$\mu$ events [33] has shown that such a detector can determine the overall normalization to about 1.5%, and hence, we ignore this source of uncertainty.

#### 1. Uncertainties due to reconstruction

The uncertainty on the efficiency of reconstruction of the event is uncorrelated between CC$e$, CC$\mu$, and NC events. This can be understood as follows. The contribution from CC$\mu$ events is mainly from the low energy events (which do not have sufficient hits to be reconstructed in the Kalman filter) as can be seen from Fig. 13.

The CC$e$ events hits distribution shows a longer tail than the others because hits arise from both the electrons as well as the hadrons in the final state. Moreover, the electron-neutrino fluxes are much softer than the muon-neutrino fluxes (the former arises only in the secondary three-body decay of the cosmic muons). This different kinematic dependence of the processes leads to different reconstruction efficiencies, as can be seen from Fig. 9.

The reconstruction efficiency for NC events is small because they do not survive the minimum number of hits (hits $\geq 3$) criterion required to reconstruct their direction, because the final-state neutrino takes away a substantial part of the available energy.

CC$e$ events have hits from both the final state electron as well as the hadrons. Although the electromagnetic shower ranges out in the (5.6 cm thick) iron plates before traversing three layers or so, the combined final state causes sufficiently many hits even at low energies to pass the selection criteria and hence, typically have a higher reconstruction efficiency. The trackless CC$\mu$ events also reconstruct better

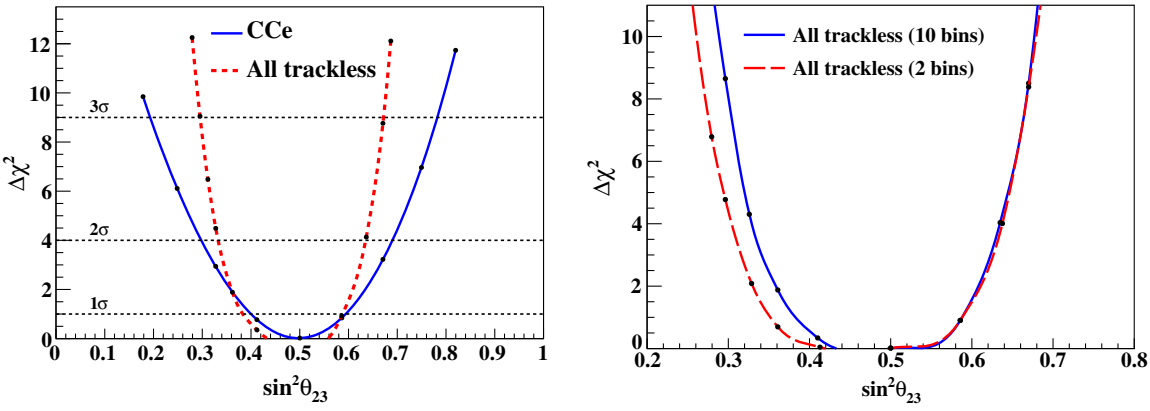


FIG. 19. Left: $\Delta\chi^2$ as a function of $\sin^2\theta_{23}$ with only CC$e$ events (solid blue lines) compared with the sensitivity when all trackless events (dotted red lines) are included. Right: $\Delta\chi^2$ as a function of $\sin^2\theta_{23}$ with all trackless events binned into ten direction bins (solid blue line) compared to the case when the number of $\cos\theta$ bins is reduced to just two (up and down) (dashed red line).

than the NC events because of hits from both the muons and the hadrons in the final state although the muon in such events has typically a low momentum and hence failed to be reconstructed as a proper track satisfying various selection criteria. The CC$\mu$ have a higher reconstruction efficiency at small values of $\cos\theta_{\rm reco}$ since overall they have a harder spectrum. (Note that NC events induced by $\nu_e$ have roughly two-thirds of the efficiency of those induced by $\nu_\mu$ for the same reason.)

While CC$e$ events also arise from a softer flux spectrum, the presence of electrons in the final state adds to the total number of hits and hence, more CC$e$ events pass these selection criteria than NC events. In any case, it can be seen that the reconstruction efficiencies of the different events contributing to the analysis have different origins and are hence uncorrelated. We therefore apply a uniform 2% systematic uncertainty on the reconstruction efficiencies but include them in the analysis as three different uncorrelated pulls, one for each channel. Note that applying *uncorrelated pulls* allows more flexibility in the fitting and hence, a more conservative estimate of the uncertainties. If the pulls were correlated, the resulting net sensitivity that we obtain below, would improve.

With the addition of these systematics, the $\chi^2$ now becomes

$$\chi^2 = \min_{\{\xi\}} \sum_i 2\left\{N_i(\xi) - D_i - D_i \ln\left[\frac{N_i(\xi)}{D_i}\right]\right\} + \xi_Z^2 + \xi_{\rm CC}^2{}_e + \xi_{CC_\mu}^2 + \xi_{NC}^2, \quad (7)$$

where the total events are given in terms of the CC$e$ ($T_i^{{\rm CC}e}$), CC$\mu$ ($T_i^{{\rm CC}\mu}$), and NC ($T_i^{\rm NC}$) events as

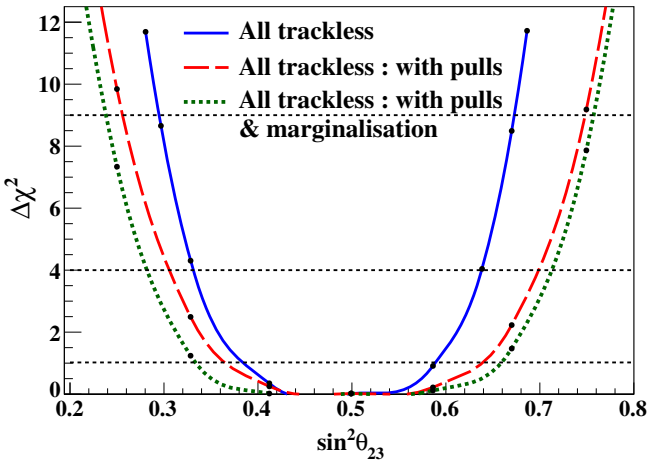


FIG. 20. $\Delta\chi^2$ as a function of $\sin^2\theta_{23}$ for all trackless events without pulls (blue solid lines), with pulls (red dashed lines) and with pulls after marginalization (green dotted lines), for an exposure of ten years, assuming a 50 kton detector.

$$N_i(\xi) \equiv \{(T_i^{{\rm CC}e} + T_i^{{\rm CC}\mu} + T_i^{\rm NC})(1 + \pi_i\xi_Z) + \pi_i^{\rm reco}(T_i^{{\rm CC}e}\xi_{{\rm CC}e} + T_i^{{\rm CC}\mu}\xi_{{\rm CC}\mu} + T_i^{\rm NC}\xi_{\rm NC})\}, \quad (8)$$

where $\pi_i$ is the correlated systematic uncertainty in the zenith-angle dependence for the different sets of events, and $\xi_Z$ is the corresponding pull. Although the same uncorrelated error $\pi_i^{\rm reco}$ is applied across all sets of events, three different pulls are applied to the CC$e$ ($\xi_T$), trackless CC$\mu$ component ($\xi_{CC_\mu}$), and NC component ($\xi_{NC}$), respectively, to account for the varying signatures of these events.

The analysis is repeated with the inclusion of uncertainties on all three types of trackless events. As expected, the sensitivity decreases, as can be seen in Fig. 20, which shows $\Delta\chi^2$ as a function of $\sin^2\theta_{23}$ with and without pulls. The results are also then marginalized over the $3\sigma$ range of the remaining neutrino oscillation parameters (excluding the solar parameters), as given in Table I and the result plotted in Fig. 20. The inclusion of systematic uncertainties as well as marginalization, reduces the relative $1\sigma$ precision on $\sin^2\theta_{23}$ from 15% to 21%.

## VI. DISCUSSIONS AND CONCLUSIONS

Simulation studies of charged-current atmospheric muon neutrino events, CC$\mu$, in the ICAL detector have established its capability to precisely determine the so-called atmospheric parameters, $\theta_{23}$ and $\Delta m^2_{32}$, including its sign (the neutrino mass ordering issue) through the observation of earth matter effects in neutrino (and antineutrino) oscillations. In this paper, for the first time, we consider the contribution to the sensitivity to atmospheric neutrino oscillation parameters from *trackless* events in the ICAL detector, where no track (typically assumed to be a muon) could be reconstructed. Such events arise from charged current electron and muon events as well as from neutral current interactions in the detector.

We used a simulated sample generated by the NUANCE neutrino generator, which corresponds to 100 years (or equivalently to 5000 kton years) of data, in which the response of ICAL is modeled by GEANT4. Using pure CC$e$ events, we first studied the simulation response of an ICAL-like detector witan h electron separation capability to CC$e$ events and showed that the detector is capable of reconstructing the energy and direction of the final state shower (of the combined electron and hadrons in the final state) with reasonable accuracy and efficiency. These reconstructed observables are then used in a $\chi^2$ analysis. It is shown that there was sufficient sensitivity to $\theta_{23}$.

However, it turns out that the ICAL will not be able to cleanly separate CC$e$ events (containing both electron and hadrons in the final state) from NC events (with only hadrons in the final state) or CC$\mu$ events (where the muon track failed to be reconstructed). While various selection criteria are applied, in particular, the number of hits per layer, to try and improve the discrimination to electron

TABLE II. Sensitivity to $\sin^2\theta_{23}$ for pure CC$e$ events, all trackless events and all trackless events with systematic uncertainties, for an exposure of ten years, assuming a 50 kton detector.

| Binning in $\cos\theta_{\text{reco}}$ | Relative $1\sigma$ precision on $\sin^2\theta_{23}$ |
|---|---|
| CC$e$ | 20% |
| All trackless | 15% |
| All trackless, including systematics and marginalization | 21% |

events, these requirements led to worse sensitivities to the oscillation parameters, since the analysis is statistics dominated. We therefore analyze the *total* collection of so-called "trackless events" arising from CC$e$, CC$\mu$, and NC events. The increased statistics as well as the known sensitivity of CC$\mu$ events to oscillation parameters changed the sensitivity to $\sin^2\theta_{23}$ significantly. We summarize our results in Table II where we show the results when the events are binned in the polar angle $\cos\theta$ alone; we also show that there is hardly any change in sensitivity when we include energy binning as well.

In summary, neutrino experiments are low counting experiments, and hence, it is important to reconstruct and analyze all possible events in neutrino detectors. A first study of the subdominant trackless events at the proposed ICAL detector at INO indicates that these will be sensitive to $\theta_{23}$ and hence need to be considered as well.

## ACKNOWLEDGMENTS

We thank Gobinda Majumder and Asmita Redij for developing the ICAL detector simulation packages. We thank the referees for several useful remarks and suggestions that greatly improved the manuscript.

[1] B. Pontecorvo, J. Exp. Theor. Phys. **6**, 429 (1958), http://www.jetp.ac.ru/cgi-bin/dn/e_006_02_0429.pdf; Z. Maki, M. Nakagawa, and S. Sakata, Prog. Theor. Phys. **28**, 870 (1962).
[2] A. Gando *et al.* (KamLAND Collaboration), Phys. Rev. D **88**, 033001 (2013).
[3] K. Abe *et al.* (Super-Kamiokande Collaboration), Phys. Rev. D **94**, 052001 (2016).
[4] F. An *et al.* (Daya Bay Collaboration), Phys. Rev. D **95**, 072006 (2017).
[5] Y. Abe *et al.* (Double Chooz Collaboration), J. High Energy Phys. 01 (2016) 163.
[6] J. H. Choi *et al.* (RENO Collaboration), Phys. Rev. Lett. **116**, 211801 (2016).
[7] M. Tanabashi *et al.* (Particle Data Group), Phys. Rev. D **98**, 030001 (2018) and 2019 update.
[8] F. An *et al.* (JUNO Collaboration), J. Phys. G **43**, 030401 (2016).
[9] S. Adrián-Martínez *et al.* (KM3NeT collaboration), J. High Energy Phys. 05 (2017) 008.
[10] M. G. Aartsen *et al.* (IceCube Collaboration) Phys. Rev. Lett. **120**, 071801 (2018).
[11] B. Abi *et al.* (DUNE Collaboration), arXiv:1807.10334.
[12] I. Esteban, M. C. Gonzalez-Garcia, M. Maltoni, I. Martinez-Soler, and J. Salvado, J. High Energy Phys. 08 (2018) 180.
[13] S. Ahmed *et al.* (ICAL Collaboration), Pramana **88**, 79 (2017).
[14] T. Thakore, A. Ghosh, S. Choubey, and A. Dighe, J. High Energy Phys. 05 (2013) 058.
[15] A. Ghosh, T. Thakore, and S. Choubey, J. High Energy Phys. 04 (2013) 009.
[16] M.-M. Devi, T. Thakore, S. K. Agarwalla, and A. Dighe, J. High Energy Phys. 10 (**2014**) 189.
[17] L. S. Mohan and D. Indumathi, Eur. Phys. J. C **77**, 54 (2017).
[18] L. S. Mohan *et al.*, J. Instrum. **9**, T09003 (2014).
[19] M.-M. Devi, A. Ghosh, D. Kaur, S. M. Lakshmi, S. Choubey, A. Dighe, D. Indumathi, S. Kumar, M. V. N. Murthy, and M. Naimuddin, J. Instrum. **8**, P11003 (2013).
[20] M.-M. Devi, A. Dighe, D. Indumathi, and S. M. Lakshmi, J. Instrum. **13**, C03006 (2018).
[21] S. Agostinelli *et al.* (GEANT4 Collaboration), Nucl. Instrum. Methods Phys. Res., Sect. A **506**, 250 (2003).
[22] J. Allison *et al.*, IEEE Trans. Nucl. Sci. **53**, 270 (2006).
[23] D. Casper, Nucl. Phys. B, Proc. Suppl. **112**, 161 (2002).
[24] D. Indumathi, M. V. N. Murthy, G. Rajasekaran, and N. Sinha, Phys. Rev. D **74**, 053004 (2006).
[25] C. Patrignani *et al.*, Chin. Phys. C **40**, 100001 (2016) and 2017 update.
[26] M. Honda, T. Kajita, K. Kasahara, and S. Midorikawa, Phys. Rev. D **83**, 123001 (2011).
[27] G. Rajasekaran, AIP Conf. Proc. **721**, 243 (2004).
[28] S. R. Dugad, Proc. Indian Sci. Acad. A **70**, 39 (2004), https://insa.nic.in/writereaddata/UpLoadedFiles/PINSA/Vol70A_2004_1_Art04.pdf.
[29] R. E. Kalman, Trans. ASME J. Basic Eng. **82**, 35 (1960).
[30] L. S. Mohan, Precision measurement of neutrino oscillation parameters at INO ICAL, Ph. D. thesis, 2014.
[31] M. C. Gonzalez-Garcia and M. Maltoni, Phys. Rev. D **70**, 033010 (2004).
[32] G. L. Fogli, E. Lisi, A. Marrone, D. Montanino, and A. Palazzo, Phys. Rev. D **66**, 053010 (2002).
[33] K. R. Rebin, J. Libby, D. Indumathi, and L. S. Mohan, Eur. Phys. J. C **79**, 295 (2019).